Temporal and Spectral Properties of Comptonized Radiation and Its Applications

Demosthenes Kazanas, Xin-Min Hua[1] and Lev Titarchuk[2]

LHEA, NASA/GSFC Code 661, Greenbelt, MD 20771

Received ______________; accepted ______________

submitted to ApJ

[1]NRC/NAS Senior Research Associate

[2]CSI, George Mason University

ABSTRACT

We have found relations between the temporal and spectral properties of radiation Comptonized in an extended atmosphere associated with compact accreting sources. We demonstrate that the fluctuation power spectrum density (PSD) imposes constraints on the atmosphere scale and profile. Furthermore, we indicate that the slope and low frequency break of the PSD are related to the Thomson depth τ_0 of the atmosphere and the radius of its physical size respectively. Since the energy spectrum of the escaping radiation depends also on τ_0 (and the electron temperature kT_e), the relation between spectral and temporal properties follows. This relation allows for the first time an estimate of the accreting matter Thomson depth τ_0 independent of arguments involving Comptonization. We present figures for the light curves and PSD of different energy bands, the photon energy spectra and the phase lags as functions of the variability frequency. The temporal properties of the high (soft) and low (hard) state of black hole sources are discussed in this context.

Subject headings: accretion— black hole physics— radiation mechanisms: Compton and inverse Compton— stars: neutron— X-rays: QPO

1. Introduction

Much of the information about the conditions in the vicinity of compact accreting objects, the region where most of the accretion kinetic energy is themalized and converted into radiation, has so far come from observations and modeling of their energy spectra. Specifically, the observations of power-law high energy ($E \gtrsim 2 - 50$ keV) spectra has established the process of unsaturated Comptonization of soft photons by hot electrons as the main process by which these spectra are produced (see e.g. Sunyaev & Titarchuk 1980). However, the spectral information alone does not suffice to determine the physical parameters of the system, since it can only determine the combination of the Thomson depth, τ_0, and the electron temperature, T_e, which is relevant to the Comptonization of soft photons by the hot electrons, namely the Comptonization parameter y defined as $y \simeq (4kT_e/m_ec^2)\tau_0^2$, for $\tau_0 \gg 1$. In this respect, one should bear in mind that for quasi-spherical, free-fall accretion, the above parameters, *i.e.* $\tau_0, \ y$, are independent of the mass of the accreting object, provided that the accretion proceeds at the same fraction of its Eddington value. Thus, in order to completely determine the physical parameters of these systems, additional, independent information is needed to set the scale of the radius and the density of the emitting region, information which can only come from the dynamics of accretion. These arguments have motivated the study of time variability of accreting sources and in particular of galactic black hole candidates; it was thought that the absence of a solid boundary in these bright sources would allow one to probe the dynamics of accretion onto the black hole.

However, the study of time variability of black hole candidate sources, in particular the archetypal galactic source Cyg X–1, has yielded a number of results which were rather unexpected when viewed within the standard framework of the viscous accretion disk model for the dynamics of matter accretion and emission of radiation from these sources:

(a) The fluctuation power spectral densities (hereafter PSD) are generally power laws of indices $s \sim 1 - 1.5$ in the variability frequency ω, *i.e.,* $|F(\omega)|^2 \propto \omega^{-s}$ for $\omega > \omega_c$ and $|F(\omega)|^2 \propto \omega^0$ for $\omega < \omega_c$ (see e.g. van der Klis 1995). The values of the slope, s, of the PSD are thus significantly flatter than these expected from exponential shots associated with the turbulent dynamics of the accreting gas near its last stable orbit ($s \geq 2$). Furthermore, the turnover frequency, ω_c, is generally several orders of magnitude smaller than those associated with the dynamics responsible for the emission of high energy radiation. For Cyg X–1, the archetypal galactic black hole candidate, $s \simeq 1$ (flicker noise), while $\omega_c \simeq 0.05$ Hz, a far cry from the kHz frequencies expected on the basis of dynamical considerations. (b) In addition to these broad band spectral features, the PSD of black hole candidates also exhibit QPO's. The observation of these features, thought to result from the "beating" between the Keplerian frequency of an accretion disk and the rotation of an underlying neutron star, poses a problem for systems thought to contain black holes. (c) The spectral – temporal studies of Miyamoto et al. (1988) of the time lags between hard and soft photons as a function of the variability frequency ω, has indicated that these lags, at least in Cyg X–1, decrease with increasing variability frequency ω, thus ruling out Comptonization by an electron cloud of uniform density and temperature.

Motivated by the discrepancy of the above systematics of time variability in black hole candidates from those expected on the basis of the "standard" dynamical models of viscous accretion disks, we present in this study an alternative model for the time dependent spectral formation of Comptonized radiation which can reproduce the basic observational features described above. In §2 we describe our model and demonstrate the relation between the PSD shapes and the slopes of the photon energy spectra; we also emphasize the nature of the white noise spectra below ω_c as well as the physics associated with the low value of this turnover frequency. In §3 we discuss the issue of the very low-frequency noise and we briefly review the relevance of the present model to RXTE observations of Cyg X-1 in its

low and high states. Finally, we discuss and summarize our results in §4.

2. The Extended Atmosphere Model

Our study uses as background the model of Chakrabarti & Titarchuk (1995; hereafter CT95), i.e. quasi-spherical accretion with a centrifugally supported shock, which thermalizes the accretion kinetic energy and gives rise to the hot electrons responsible for the Comptonization of soft photons. However, we postulate, in addition, that the quasi-spherically accreting component behaves like a hot "atmosphere" of constant electron temperature $T_e \sim 50$ keV and, more importantly, with a density profile $n(r) \propto 1/r$ in radius, extending to $r = r_c \simeq 10^4 \;\; R_s$, where $R_s = 2GM/c^2$ is Schwarzschild radius. This atmosphere is thought to be the result of preheating of the accretion flow by the radiation produced at the shock, as discussed by Zeldovich & Shakura (1969) and Chang & Ostriker (1985 and references therein) (see additional discussion on the issue of this specific density profile in §4).

We assume, for simplicity, that the geometry of this configuration is spherical and that there is a source of soft photons within the spherical shock boundary of radius $r_{\rm sh}$. The electron density is considered to be constant, n_+, inside this boundary and $n_+ r_{\rm sh}/4r$ in the atmosphere outside. The discontinuity of a factor 4 in density across the boundary $r_{\rm sh}$ is to account for the density jump across the shock. The physical size of this cloud is determined by the total optical depth τ_0. We have calculated the response of this configuration, i.e. the region interior to the shock plus the extended atmosphere, to an impulsive input of soft photons within the radius of the shock. The calculations were carried out by a modified Monte Carlo code based on the method described in Hua & Titarchuk (1995). Figures 1a and 1b show the resulting light curves at different energy bands for clouds with $\tau_0 = 1, 2$ and 3, $n_+ = 1.6 \times 10^{17}$ cm^{-3}, $r_{\rm sh} = \tau_0 \times 10^{-4}$ light seconds and outer radius of the atmosphere

$r_c = 5 \times 10^3 r_{\rm sh} \simeq \tau_0$ 0.5 light seconds. It is apparent that their shapes have the form of power laws over the time range 10^{-3} s to ~ 1 s, followed by an exponential cutoff at times of order a few seconds. For comparison, the exponential light curves from a cloud with uniform density $n = 2 \times 10^{14}$ cm^{-3}, radius $r = 1.5 \times 10^{10}$ cm ($\simeq 0.5$ light seconds) the same electron temperature T_e and $\tau_0 = 2$ are also shown (dotted curves).

The power law form of the light curves, $f(t)$, is the result of photons scattering in the extended atmosphere whose optical path has a logarithmic radial dependence

$$\tau = \int_0^r \sigma_T n_e dr \;\; = \;\; \tau_{\rm sh}[1 + 0.25 \cdot \ln(r/r_{\rm sh})] \quad \text{for} \;\; r \geq r_{\rm sh} \tag{1}$$

where the electron density $n_e = n_+$ for $r \leq r_{\rm sh}$ and $n_+ r_{\rm sh}/4r$ for $r \geq r_{\rm sh}$; σ_T and $\tau_{\rm sh}$ are the Thomson cross section and optical thickness of the shock respectively. In the case that the optical depth of the extended atmosphere is a few, most photons escape either unscattered or after one scattering (we exclude in these considerations the photon spread in time over the short time scales $\sim r_{\rm sh}/c$ associated with the uniform sphere at the center of radius $r_{\rm sh}$). The light curves of figure 1 present the distribution in the delay times of the escaping photons with respect to the light crossing time, for photons which have scattered once. The light curve is related to the distribution of photons over the time of the first scattering t_1. The probability of scattering in an interval between t_1 and $t_1 + dt_1$ is $P(t_1)dt_1 = f(\tau)d\tau$ where $f(\tau)$ is the probability density to scatter between depths τ and $\tau + d\tau$. In our case this probability density is constant and equal to $1/\tau_0$, *i.e.* inversely proportional to the total depth of the atmosphere. Therefore,

$$P(t_1) = \frac{1}{\tau_0}\frac{d\tau}{dt_1} = \frac{1}{\tau_0}\frac{d\tau}{dr}\frac{dr}{dt_1} = \frac{1}{\tau_0}\sigma n_e(r)c \tag{2}$$

For a density distribution which is a power law, *i.e.* $n_e(r) \propto r^{-\alpha}$ (we herein consider the case $\alpha = 1$) $P(t_1) \propto t_1^{-\alpha}$. One can establish, by looking at the geometry of photon trajectories in a spherical geometry of radius R, that for a photon which has scattered at

radius r_1 the average distance before escape is given by

$$\langle \ell \rangle = \frac{1}{2} r_1 \left[\frac{R}{r_1} + \frac{1}{2} \left(\frac{R^2}{r_1^2} - 1 \right) \cdot \ln \left(\frac{R + r_1}{R - r_1} \right) \right] \ ,$$

indicating that for small values of r_1 the average delay time t_d of photon escape after one scattering relative to the light crossing time of the entire atmosphere of size R is

$$\langle t_d \rangle = r_1 \left(1 - \frac{r_1}{3R} \right) \simeq r_1 \ . \tag{3}$$

The linearity between the scattering time t_1 and the delay time t_d allows us to substitute t_d in equation (2) above, leading to a light curve which is a power law in t (or better in t_d) with index equal to that of the density profile index α.

The Monte Carlo calculations shown in figure 1 support the arguments presented above. The slope of the the light curve for the uniform sphere of small scattering depth is close to zero (dotted curve) and that of the atmosphere considered here is close to -1; we have also used a density distribution appropriate to free-fall *i.e.* $n(r) \propto r^{-3/2}$ with results in accordance with the above arguments. It is well known (Sunyaev & Titarchuk 1985) that for photons escaping from a source of finite size, the distribution of number of scatterings is an exponential i.e. $f(u) \propto \exp(-\beta u)$, where u is the scattering number and the parameter β is inversely proportional to the mean number of scatterings, $\hat{u}$, which is greater than 1 for clouds with total optical depth $\tau_0 \gtrsim 1$. Thus, as expected on the basis of this argument, the light curve has an exponential turnover at delays longer than $1/\beta$ times the scattering time at the largest decade of radius. These arguments therefore present the possibility that measuring these light curves, e.g. by computing the resulting PSDs, can provide *a tool for uncovering the density profile of the atmosphere* .

As the optical depth of the atmosphere increases, multiple scattering (diffusion) effects in the extended atmosphere become more important and the above arguments, which rely on the single scattering approximation, have to be reformulated. The power law indices of

the light curves evolve to smaller values; in fact, in the uniform sphere case and for very large optical depths, as well known, the light curves become rising in time (see e.g. Hua & Titarchuk 1996; hereafter HT96). The flattening of the light curves is indicated clearly in our our Monte Carlo calculations presented in figures 1a and 1b. This change in the light curve slopes reflects directly on the resulting PSD spectra, shown in figures 1c and 1d. It can be seen there that the PSD curves are also power laws in Fourier frequency ω, since the Fourier transformation of a power-law, $t^{-\alpha}$, is also a power-law in frequency $\omega^{\alpha-1}$. Thus the flattening of the light curves leads to steepening of the PSD spectra, which however, as a rule, are flatter than those corresponding to the PSD of a uniform source ($\propto \omega^{-2}$; dotted curves), which correspond to exponential-shot light curves.

Assuming that the temperature of the extended "atmosphere" is constant, a change in its total optical depth τ_0, which results in a change of the light curve index and a steeper PSD, will manifest itself, in addition, in the energy spectrum of the escaping radiation: The increase in optical depth will lead to a harder energy spectrum for the emerging photons. Therefore, our considerations, supplemented by the Monte Carlo calculations, support to the conclusion that, under the assumption of the existence of an "atmosphere" with the density profile described above, *there should exist well defined correlations between the slopes of the escaping photon spectra and those of the PSD*. We believe that RXTE is uniquely suited to search and document the presence of such correlations.

In Figure 2 we plot the energy spectrum (solid curve) resulting from the extended atmosphere with parameters $kT_e = 50$ keV and $\tau_0 = 3$. It is seen that it is almost identical to that from a uniform plasma cloud with the same electron temperature T_e but a different optical thickness $\tau_0 = 2$ (dashed curve). For comparison, we also plot the energy spectrum from a uniform cloud with the same temperature and $\tau_0 = 3$ (dotted curve). It is seen that this spectrum is harder than the other two. This is because for the same total optical

thickness ($\tau_0 = 3$), photons in the uniform cloud find it harder to escape than those in the $1/r$ atmosphere. This example shows clearly that spectroscopic analysis alone can not provide complete information about the source structure and to get a complete picture of the spectral formation it is necessary to analyze in conjunction the temporal as well as the spectral data.

The time information is of course of vital importance for setting the physical scale of the system. Since it is believed that Comptonization is the main mechanism for the production of X-rays, measurements of the time lags between two different energies in the X-ray band should give us a direct estimate of the density of the region at which Comptonization takes place. Based on simple arguments concerning the dynamics of accretion onto compact objects, the associated time lags are expected be of the order of msec for galactic objects. It is worth noting that, for the uniform density hot clouds considered almost exlusively todate in the literature, the time lags between soft and hard photons are constant and independent of the Fourier frequency ω. Extensive caculations of this type (*i.e.* of scattering in clouds of uniform density) are given in HT96. For the non-uniform density profile of the extended atmosphere discussed herein, the shape of the phase lag as a function of the variability frequency ω also changes. In Figure 3, we plot the phase lags of photons in the $10 - 20$ keV band relative to those in $1 - 10$ keV band, for the four cases depicted in Figure 1, as a function of ω. As in Figure 1, the dotted curve corresponds to the configuration of the uniform cloud described earlier and its shape is similar to those displayed in Figures $14 - 17$ of HT96, except that here the curve extends to higher frequencies with a roughly constant slope instead of a sharp drop. This is because in present analysis we use much finer time bins than before. However, the maximum at frequency $\sim n_e \sigma_T c/\tau_0$ (HT96, Eq. 11) is clear and sharp. On the other hand, the phase lags corresponding to the $1/r$ atmosphere configuration (solid curves) are much flatter and there is no maximum present across the entire range of frequencies. It is interesting to point out that this type of phase lag is hinted

in the GINGA observations of Cyg X-1 (Miyamoto et al. 1988) and also seen in the recent observations of the high state of Cyg X-1 (Swank et al. 1996).

As pointed out in HT96, the PSD associated Comptonized photons of a given energy, depends strongly on the energy of the source, soft photons. In Figure 1, the source photons have a blackbody temperature 2 keV. In Figure 4, we present the PSD curve (solid curve) in the energy range 10 – 20 keV resulting from the same configuration as that of $\tau_0 = 2$ in Figure 1, but with the source photons at blackbody temperature $kT_0 = 0.5$ keV. Compared to the corresponding PSD curve in Figure 1, it is seen that PSD with lower source photon energy is steeper, in agreement with the analysis of HT96.

In Figure 4, we also present one more PSD (dotted) curve, corresponding to the same light curve as the solid one but for different time ranges and time bins. For the solid curve the light curve is calculated over a range of 4 seconds in 4096 bins. For the dotted curve, the light curve is calculated over 32 seconds in the same number of bins. It is seen that the PSD turns flat for frequencies below $\omega_c \sim 0.25$ Hz while keeps parallel to the solid one above ω_c except at the highest frequency end, which is obviously due to aliasing (see e.g. Press et al. 1992). It is found from examining the light curve that the time scale corresponding to $1/\omega_c = 4$ seconds is actually the time scale of the light curve beyond which the latter drops virtually to zero. Thus we have found a possible physical meaning for the shoulder (break) frequency ω_c in the PSD curves, which is common in the PSD of many sources, namely, it indicates the time scale of the light curve, or alternatively the size of the extended $1/r$ atmosphere. The "white noise" below ω_c reflects the average frequency of the shots while the power-law above ω_c reflects the time structure within one single shot.

3. The very low frequency noise

In addition to the fluctuation PSD described above, galactic X-ray sources exhibit power-law type PSD at frequencies much lower than ω_c, so that the white noise component at $\omega < \omega_c$ appears only as a shoulder in the much broader PSD spectrum. We have thus reasons to believe that this very low frequency component in the PSD is separate from the one described above. One should bear in mind that at radii $r \gg r_c$, related to the dynamics associated with this component in the PSD, the effects of preheating are thought to be small and accretion proceeds in the form of the standard viscous α-disk (Shakura & Sunyaev 1973 hereafter SS73). As a result, one can consider the fluctuations in the accretion rate $\dot{M} = \dot{M}_0 + \delta\dot{m}$ to be resulting from small random variations in the viscosity parameter α, *i.e.* $\alpha = \alpha_0 + \delta$. This model was considered by Lyubarskij (1995), who, by solving the angular momentum diffusion equation, showed that the resulting accretion rate and hence the luminosity, has a flicker-type fluctuation spectrum, provided that the characteristic time of the fluctuations in α are of the order of the viscous time scales, and the fluctuations in α at different radii are uncorrelated.

We provide here a heuristic derivation of this fact for the sake of completeness of the discussion. The accretion time τ_a from a radius r in an α-disk is

$$\tau_a = \left[\alpha \left(\frac{h}{r}\right)^2 \Omega_K\right]^{-1} . \tag{4}$$

The variation δ in the viscosity parameter α in an annulus leads to the mass accretion rate variations $\delta\dot{m}_i \propto \delta(r,t)$. In fact the contribution in the mass variation caused by the viscosity variations is proportional to the annulus area rdr, the surface density u and inversely proportional to the accretion time τ_a *i.e.*,

$$\delta\dot{m}_i \propto \frac{\delta \cdot urdr}{\tau_a} . \tag{5}$$

In different accretion disk regions (SS73) (region **a**: $p_r \gg p_g$ and $\sigma_T \gg \sigma_{ff}$, region **b**: $p_r \ll p_g$ and $\sigma_T \gg \sigma_{ff}$, region **c**: $p_r \ll p_g$ and $\sigma_T \ll \sigma_{ff}$) there are different dependences of the surface density u and thickness of disk H on radius. For region **a**, $u \propto r^{1.5}$, H is almost constant and hence $\tau_a \propto r^{3.5}$ (see Eq. 4) ; for region **b**, $u \propto r^{-0.6}$, $H \propto r^{21/20}$ and $\tau_a \propto r^{1.4}$; for region **c**, $u \propto r^{0.75}$, $H \propto r^{9/8}$ and $\tau_a \propto r^{3.5}$. Despite the differences in the behavior of the main parameters over the disk one can check by substituting the above expressions of u, H and τ_a in Eqs. 4 and 5 that the mass (or luminosity) variations are the same for all zones **a-c**, namely

$$dL \ \propto \ d\dot{m}_i \ \propto \ \frac{dr}{r} \ \propto \frac{d\tau_a}{\tau_a} = \frac{d\omega}{\omega} \tag{6}$$

and thus the resulting power spectrum $p(\omega)$ is

$$p(\omega) \ \propto \ \omega^{-1}. \tag{7}$$

In other words if the amplitude of the variations in α are the the same at different radii then the amplitudes of accretion rate (luminosities) variations are the same at different time scales (Lyubarskij 1995).

4. Discussion and Conclusion

We have presented above a model which implies corelations between the spectral and temporal properties of accreting compact objects and have pointed out that this relation, along with independent measurements of the electron temperature T_e, can allow a complete specification of the physical parameters of these systems, including the density profile of the extended atmosphere.

Much of the present discussion relies on the specific form of the density $n(r)$ of the accreting matter as a function of radius r. Clearly, this is not the free-falling solution customarily used in association with spherically symmetric accretion, so a few comments

are in order. If the presence of the extended atmosphere is due to the effects of preheating, as suggested in §1, then at the edge of this atmosphere, at $r \simeq r_c$, one would expect the random and rotational velocities of matter to be comparable and that the subsequent evolution of the accreting fluid in radius to be predominantly governed by the removal of its angular momentum. The agent responsible for this process is considered herein to be the interaction of the fluid with the photons produced at the base of the extended atmosphere, *i.e.* near the Schwarzschild radius R_s. In order to estimate the effectiveness of this process we compare the free-fall time scale, t_{ff}, with that of the viscous time scale, t_{visc}, assuming that the density has the required profile. Assuming that the density profile of the atmosphere has the form $n(r) = n_0(r_0/r)$ between radii r_0 and r_c, with $r_c \sim 10^3 - 10^4\ r_0$, mass conservation dictates that the the infall velocity, $v(r)$, will also have a similar scaling between r_0 and r_c, *i.e.* $v(r) = v_0(r_0/r)$, yielding for the free-fall time $t_{ff} \simeq r/v(r) = r^2/v_0 r_0$. The photons can achieve the required angular momentum removal if $t_{ff} \simeq t_{visc}$.

Under the assumed density and velocity scalings, the angular momentum of the fluid at a radius r would be $\mathcal{L} \simeq m_p n(r) v(r) r \cdot r^3$. This fluid interacts and transfers its angular momentum to photons diffusing from the interior regions of the atmosphere which carry substantially smaller angular momentum. The specific density profile we have assumed, which implies an equal optical depth per decade of radius, guarantees that: (a) The angular momentum of the photons, as they traverse each decade in radius, is much smaller than the local angular momentum of the fluid. (b) The photons interact with the fluid at every decade in radius with probability ~ 1 before their escape, carrying away angular momentum at a rate $\dot{\mathcal{L}} \simeq (L/c^2) v(r) r$, where L is the total luminosity of accretion. The viscous time scale for the fluid at radius r is then the time required for the fluid at radius r to get rid of its angular momentum, *i.e.*,

$$t_{visc} \simeq \frac{\mathcal{L}}{\dot{\mathcal{L}}} \simeq \frac{n(r)c^2r^3m_p}{L} \tag{8}$$

The luminosity L is given simply by the total accretion rate $\dot{M}$ and the innermost radius of the accretion disk r_i, *i.e.* $L \simeq \beta \dot{M} c^2 (R_s/r_i) \simeq \beta m_p n_0 v_0 r_0^2 c^2 (R_s/r_i)$ with the parameter β allowing for accretion onto the compact object other than that associated with the spherically accreting component (most likely associated with a viscous geometrically thin disk). Substituting the expression for L onto equation (8) above yields for the viscous time scale

$$t_{visc} \simeq \frac{r^2}{v_0 r_0} \frac{1}{(R_s/r_i)\beta} = t_{ff} \frac{1}{(R_s/r_i)\beta} \tag{9}$$

The above expression indicates that the removal of the angular momentum of the accreting matter by the photons produced near $r \simeq R_s \ll r_c$ can in fact proceed on dynamical time scales and thus preserve the assumed density profile provided that $(R_s/r_i)\beta \simeq 1$, *i.e.* that the total accretion rate (including an additional component, most likely from an accretion disk) is $\simeq (r_i/R_s)$ times that associated with the spherically symmetric component. We reiterate that, most likely, this process is possible only for the density profile prescribed above ($n(r) \propto 1/r$), since this is the only profile which allows for significant photon scattering, and hence removal of angular momentum, from a large range of radii.

The presence of the extended atmosphere discussed above, due presumably to upstream heating of the accreting matter, may bear relevance not only to accreting black holes as discussed herein, but also to accreting neutron stars, with the overall similarity of their PSD spectra (Van der Klis 1995) not being simply coincidental. It is interesting to speculate that coherent oscillations of this configuration (the extented atmosphere) may in fact be related to the QPO phenomenon, a phenomenon prevalent among all members of the more general class of accreting compact sources, whether neutron stars or black holes. The observed QPO frequencies are generally smaller than those associated with the dynamical motions

near a black hole or a neutron star, and similar to those associated with the outer radius r_c of our model, implying the possible relevance of this characteristic time scale in these systems too. This model may also bear relevance to the recently discovered kHz QPO's in four LMXBs (Strohmayer *et al.* 1996, Zhang *et al.* 1996), as this is the time scale expected for variability in the centrifugally supported shock presumably present at the base of the extended atmosphere, especially in objects containing neutron stars rather than black holes (Titarchuk & Lapidus 1996).

The presence of a reflection-by-cold-matter component and fluorescent K_α line emission in the observed spectra of black hole candidates and AGNs (e.g. Ebisawa et al 1996) could also be related with an extended atmosphere of the type discussed above: A significant fraction of hard photons can in the present case random walk over the entire extended atmosphere and the possibility arises that it can be reflected by far-away, relatively cold parts of the visous accretion disk to produce the required components.

In addition to the above and in accordance with the model of CT95, one would expect a variation in the temporal properties of accreting compact sources while at their different spectral states. As discussed by CT95, the changes in the spectral states derive from the presence of a sufficiently large number of soft photons from the viscous accretion disk to cool the electrons to temperatures at which Comptonization is ineffective. This manifests as a prominent thermal-like peak at energies ~ 1 keV. Under the same conditions, one could expect the extended hot atmosphere to be absent, a fact which should manifest itself in the associated PSD by the absence of power at the lowest frequencies.

We have presented above a model which implies the existence of a correlation between the temporal and spectral properties of accreting compact sources. Our model is consistent with certain general characteristics associated with the PSD of accreting compact sources observed to date, in particular with their spectral forms and the breaks associated with the

low frequency turn-overs. It is also consistent with the observed frequency dependent phase lags between photons of different energies and can also account for their photon spectra. This model is specific enough that we believe can it be meaningfully tested by combined spectal - temporal measurements of these sources.

The authors acknowledge support by NASA grants NAS-5-32484 and the RXTE Guest Observing Program. They would also like to thank Lorrela Angelini and Jean Swank for informative discussions. XMH would like to thank NAS/NRC for support during the course of this study.

REFERENCES

Chakrabarti, S., & Titarchuk, L. 1995, ApJ, 455, 623

Chang, K.M. & Ostriker, J.P. 1985, ApJ, 288, 428

Ebisawa, K., Ueda, Y., Inoue, H., Tanaka, Y. & White, N.E. 1996, ApJ, 467, 419

Hua, X.-M. & Titarchuk, L. 1995 ApJ, 449, 188.

Hua, X.-M. & Titarchuk, L. 1996 ApJ, 469, 280 (HT96)

Lyubarskij, Yu., 1995 submitted to MNRAS

Miyamoto, S. et al., 1989, Nature, 342, 773

Press, W.H., Teukolsky, S.A., Vetterling, W.T. & Flannery, B.P. 1992, Numerical Recipes (University Press, Cambridge)

Shakura, N. I. & Sunyaev, R. A. 1973, A&A, 24, 337 (SS73)

Sunyaev, R. A. & Titarchuk, L.G., 1980, A&A, 86, 121 (ST80)

——— 1985, A&A, 143, 374 (ST85)

Strohmayer, T. E., Zhang, W., Swank, J. H., Smale, A., Titarchuk, L., Day, C., & Lee, U. 1996, ApJ L, in press

Swank, J. H. et al. 1996, ApJ L, in preparation

Titarchuk, L., & Lapidus, I. 1996, ApJ L, submitted

van der Klis, M. 1995, in: X-ray Binaries, eds. W. Lewin, J. Van Paradijs and E. Van Den Heuvel (University Press, Cambridge) p. 252

Zeldovich, Ya., & Shakura, N., 1969, AZh, 46, 225 (English in Sov. Astronomy 13, 175)

Zhang, W., Lapidus, I.I., White, N. E. & Titarchuk, L. G. 1996, ApJ L, in press

This manuscript was prepared with the AAS LATEX macros v4.0.

Fig. 1.— The light curves and PSD for the extended atmosphere of temperature $kT_e = 50$ keV described in the text. Three cases of total Thomson optical depths $\tau_0 = 1, 2$ and 3 are shown. The electron density has the form $0.25 n_+ r_{sh}/r$ for radius $r > r_{sh}$ and n_+ for $r \leq r_{sh}$, where $n_+ = 1.6 \times 10^{17}$ cm^{-3} and $r_{sh} = \tau_0 \times 10^{-4}$ light seconds. For comparison, the cloud with uniform density $n = 2 \times 10^{14}$ cm^{-3} with the same temperature and $\tau_0 = 2$ is also shown (dotted curves). The left two panels show the light curves and PSD for emissions in the energy range $1 - -10$ keV, while the right two panels for $10 - -20$ keV.

Fig. 2.— Comparison of the energy spectra of emissions from uniform clouds and extended atmospheres with the same temperature and optical depth $\tau_0 = 3$. The solid curves indicate the energy spectrum resulted from same extended atmospheres as in Figure 1. The dotted curves indicate those from uniform clouds. The spectrum resulting from an extended atmosphere of $\tau_0 = 3$ (solid curve) is almost indistinguishable from that of a uniform cloud with $\tau_0 = 2$ (dashed curve). Both spectra have the same parameter $\beta = 0.334$ although they have different τ_0.

Fig. 3.— The hard X-ray phase lags resulting from the same atmospheres as in Figure 1. The dotted curve indicates the phase lag resulted from a cloud with $\tau_0 = 2$ and uniform density $n = 2 \times 10^{14}$ cm^{-3}.

Fig. 4.— The power spectra resulting from the same shot light curve but different time ranges. The emissions are from an extended atmosphere with $\tau_0 = 2$ and $kT_e = 50$ keV. The density profile is similar to the one with $\tau_0 = 2$ in Figure 1, but with source photons at blackbody temperature 0.5 keV. The solid curve represents a time range of 4 seconds while the dotted curve for 32 seconds.

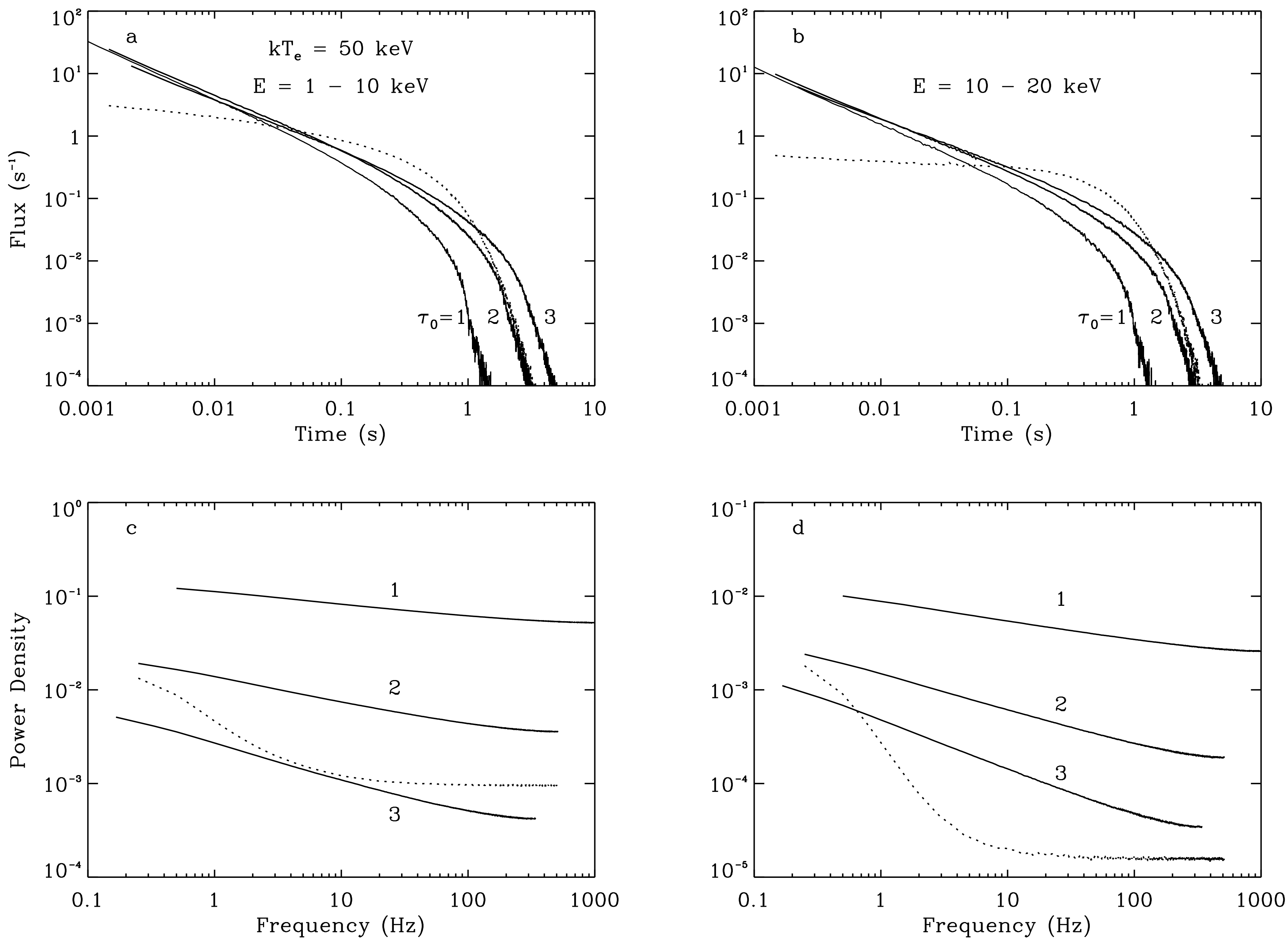

a
kT_e = 50 keV
E = 1 – 10 keV
τ_0=1
2
3
Flux (s^{-1})
Time (s)
b
E = 10 – 20 keV
τ_0=1
2
3
Time (s)
c
1
2
3
Power Density
Frequency (Hz)
d
1
2
3
Frequency (Hz)

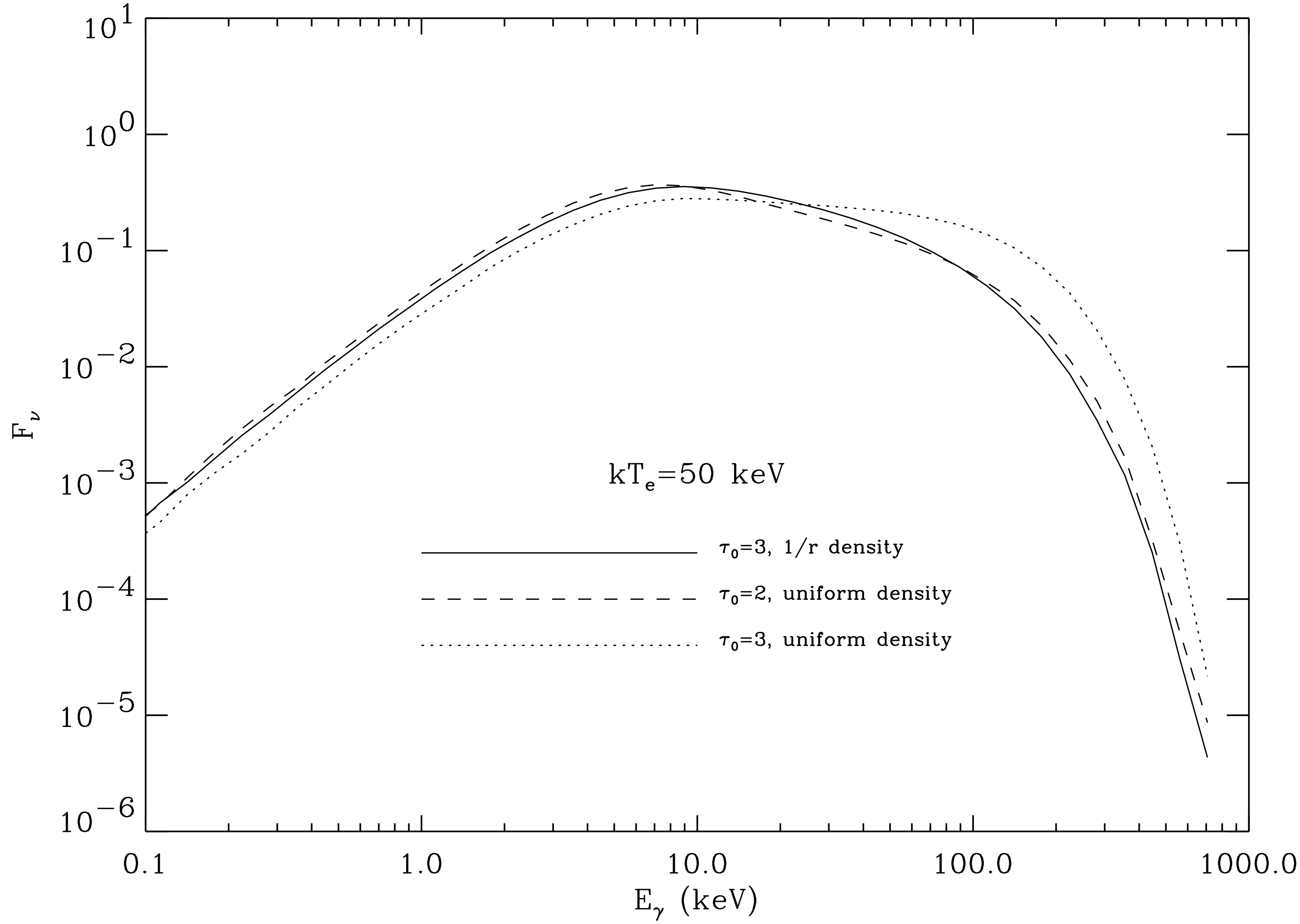

10^1
10^0
10^{-1}
10^{-2}
10^{-3}
10^{-4}
10^{-5}
10^{-6}
F_ν
kT_e=50 keV
τ_0=3, 1/r density
τ_0=2, uniform density
τ_0=3, uniform density
0.1
1.0
10.0
100.0
1000.0
E_γ (keV)

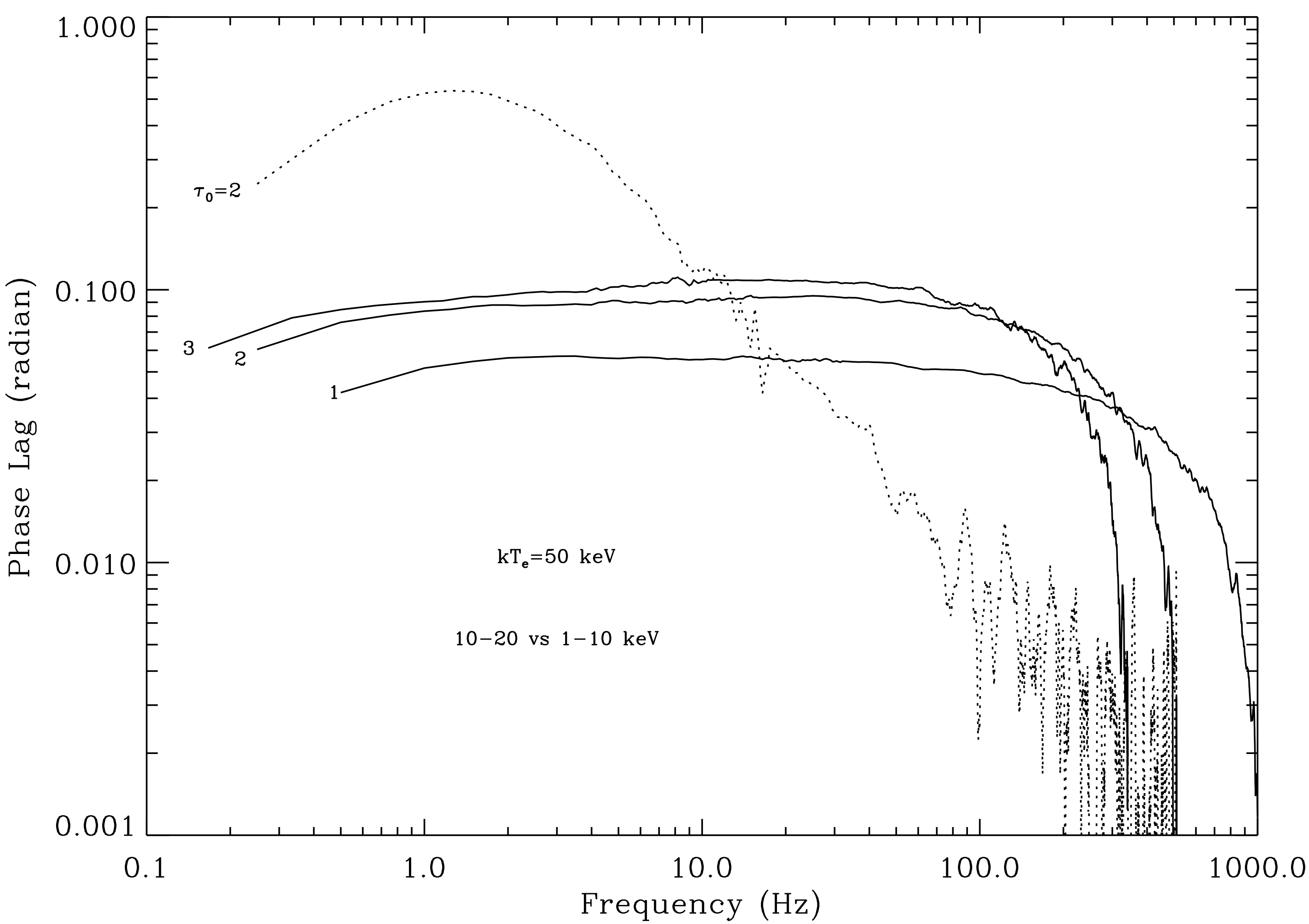

τ_0=2
3
2
1
kT$_e$=50 keV
10–20 vs 1–10 keV
Phase Lag (radian)
1.000
0.100
0.010
0.001
0.1
1.0
10.0
100.0
1000.0
Frequency (Hz)

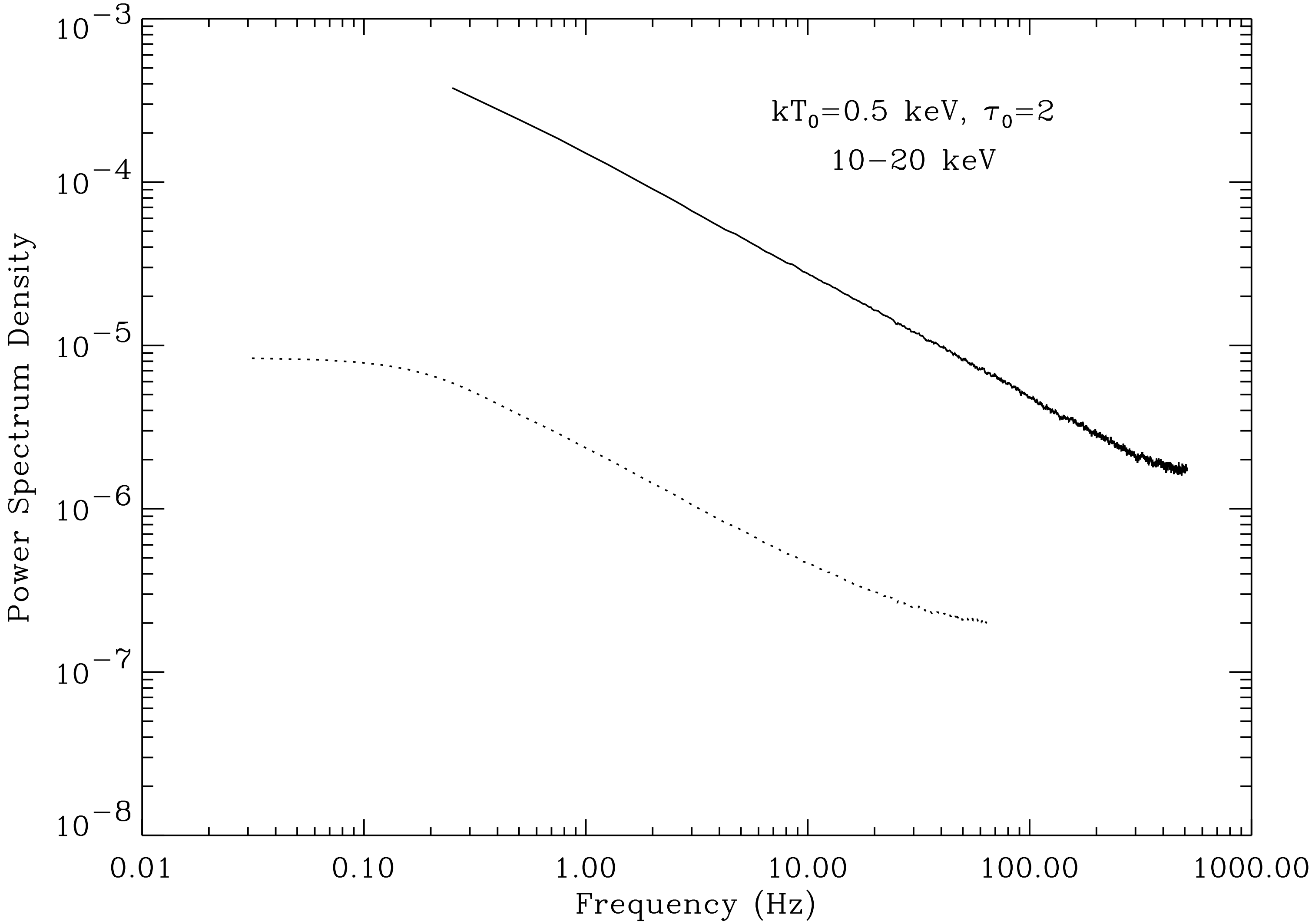

kT_0=0.5 keV, τ_0=2
10–20 keV
Power Spectrum Density
10^{-3}
10^{-4}
10^{-5}
10^{-6}
10^{-7}
10^{-8}
0.01
0.10
1.00
10.00
100.00
1000.00
Frequency (Hz)